Quantum interference induced by multiple Landau-Zener transitions in a strongly driven rf-SQUID qubit

Yiwen Wang,[1] Shanhua Cong,[2] Xueda Wen,[1] Cheng Pan,[1] Guozhu Sun,[2,*] Jian Chen,[2] Lin Kang,[2] Weiwei Xu,[2] Yang Yu,[1,†] and Peiheng Wu[2]

[1]*National Laboratory of Solid State Microstructures and Department of Physics, Nanjing University, Nanjing 210093, China*
[2]*Department of Electronic Science and Engineering, Research Institute of Superconductor Electronics, Nanjing University, Nanjing 210093, China*

We irradiated an rf superconducting quantum interference device qubit with large-amplitude and high-frequency electromagnetic field. Population transitions between macroscopic distinct quantum states due to multiple Landau-Zener transitions at energy-level avoided crossings were observed. The qubit population on the excited states as a function of flux detuning and microwave power exhibits interference patterns. Some features are found in the interference and a model based on rate equations can well address these features.

Coherent quantum dynamics of superconducting Josephson qubits driven by weak external field have been extensively investigated recently.[1–6] In these experiments microwave (MW) with frequency close to the energy-level separation were applied to the qubits, generating Rabi oscillations to probe the macroscopic quantum coherence in time domain. On the other hand, quantum coherence can also be investigated by applying a large-amplitude field with a relatively small frequency, driving the qubit throughout the energy-level diagram. During the sweeping process the quantum evolution is generally adiabatic except at each level crossing, where Landau-Zener (LZ) transitions occur with finite probability.[7,8] Consecutive LZ transitions give rise to Stuckelberg or Ramsey-type oscillations[9,10] in analogy to Mach-Zehnder (MZ) interferometer. Therefore, the MZ-type interference serves as a unique quantum coherence signature complementary to Rabi oscillation.

Great efforts have been made to demonstrate coherent dynamics of superconducting qubits in the strongly driven regime dominated by LZ transitions with emphasis upon two level systems.[11–15] A recent work made a step forward.[16] A superconducting flux qubit, which can be thought of as a multilevel artificial "atom," was driven through several regimes characterized by various level crossings. The applied microwave frequency was generally much smaller than the instantaneous energy-level separation. Therefore the individual photon resonance was undistinguishable. However, the qubit population under large-amplitude fields exhibited a series of diamondlike interference patterns in the space parameterized by dc flux detuning and microwave amplitude. Spectroscopic information was obtained from the field amplitude dependence of the qubit population.[17] This experiment was done with a superconducting persistent-current qubit, a niobium superconducting loop interrupted by three Josephson junctions.

Comparing with a superconducting persistent-current qubit, an rf superconducting quantum interference device (SQUID) qubit has a much larger loop size (usually 100 times larger in loop area) in order to provide the required geometrical inductance. Therefore the rf-SQUID qubit is much more sensitive to the external flux noises that induce fluctuations of energy-level separation between flux states in different wells, resulting a relatively short decoherence time (~ 1 ns). In order to observe LZ interference in such a system, the time interval between subsequent LZ tunneling events should be less than the relevant coherence time, suggesting the requirement of a high-frequency field. In a previous work,[18] we observed the quantum interference fringes in an rf-SQUID qubit due to LZ transitions at one avoided level crossing. In this paper, we report the simultaneous presence of two-set of interference fringes associating with LZ transitions at two nearby avoided crossings. In addition, the qubit population is an oscillatory function of the field amplitude at certain dc flux detuning. A model based on rate equations can well address the experimental features.

Our device with $Nb/AlO_x/Nb$ junctions was fabricated on an oxidized Si substrate by using the standard trilayer process. As shown in Figs. 1(a) and 1(b), the rf-SQUID qubit is essentially a superconducting loop with a second-order gradiometric configuration, interrupted by a small superconducting loop (barrier loop) consisting of two junctions in parallel. For external magnetic flux Φ_f^q close to $\Phi_0/2$ applied to the qubit loop, where Φ_0 is the flux quantum, the system potential exhibits a double-well landscape. The flux states in different wells, corresponding to macroscopic circulating currents flowing in opposite directions, can serve as the qubit states. Two on-chip current bias lines supply the magnetic flux to the qubit loop (Φ_f^q) and barrier loop (Φ_f^{CJJ}), detuning the potential from symmetric point and modulating the potential barrier height, respectively. Therefore, we can control two degrees of freedom of the system potential *in situ* by adjusting Φ_f^q and Φ_f^{CJJ}. An additional on-chip current bias line is used to apply microwave pulses. The qubit flux state is detected by a dc-SQUID inductively coupled to the qubit loop. We properly bias the readout dc-SQUID with an external magnetic flux (Φ_f^{dc}) in order to read out the qubit states with maximum sensitivity.

The sample was mounted on a chip carrier enclosed in a superconducting aluminum sample cell that is thermally anchored to the mixing chamber of a dilution refrigerator with a base temperature about 20 mK. The dewar was magnetically shielded by multilayer mu-metal shielding. All electri-
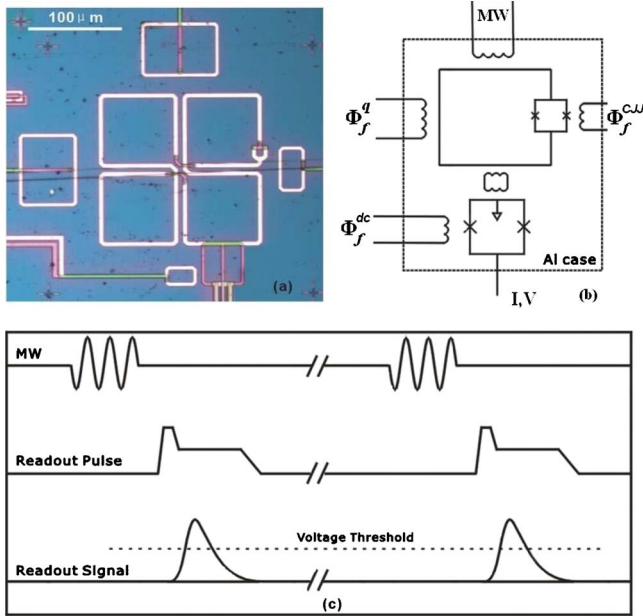
FIG. 1. (Color online) (a) Optical micrograph of the rf-SQUID qubit together with control and readout circuit. (b) Equivalent circuits of the sample layout. Crosses represent the Josephson junctions. (c) The measurement time sequence.

cal leads connected to the sample were carefully filtered and attenuated at low temperatures to minimize circuit noise (see Ref. 19 for detailed circuit description).

In this experiment, we biased Φ_f^{CJJ} at a fixed value at which the potential barrier is much higher than the intrawell energy-level separation. Therefore, there are several localized flux states in both potential wells. The interwell transition rate between the two lowest flux states of different potential wells is very small (~ 1 ms) for the flux detuning $\delta\Phi_f^q = \Phi_f^q - \Phi_0/2$ close to 0. The time sequence of measurement is shown in Fig. 1(c). For each measurement cycle, a 10 μs microwave pulse was applied to the qubit loop to induce sinusoidal excursions through the energy levels around a dc flux detuning $\delta\Phi_f^q$. At the end of microwave pulse, the qubit relaxed quickly back to the corresponding lowest state in the well since the intrawell relaxation time is very short (~ 1 ns). Then the readout pulse, consisting of a 15 ns sampling current with amplitude close the critical current and a 15 μs holding current just above the re-trapping current of the dc-SQUID, was applied to the dc-SQUID. By properly selecting the magnitude of the sampling current, the readout dc-SQUID either switched to finite voltage state or stayed at zero voltage state, depending on whether the qubit being in left well $|L\rangle$ state or in right well $|R\rangle$ state. The period of one measurement cycle was 0.2 ms. Although the measurement repetition rate is larger than the interwell thermalization rate at small flux detuning, this does not affect our resonant peaks (dips) since the long MW pulse can induce multiple LZ transitions and finally generate a stationary qubit population in the two wells. By repeating the trials for 4 $\times 10^4$ times, we obtained the average switching probability, representing the population in $|L\rangle$ state. As changing the flux detuning and microwave power step by step, we measured

the qubit population in $|L\rangle$ state as a function of flux detuning and microwave power.

In Fig. 2(a) we plotted the qubit population as a function of the flux detuning in the absence and presence of microwave irradiation. Without applying microwave, around the symmetric point of the flux detuning, the population transfer monotonically from $|L\rangle$ to $|R\rangle$, depending on which sate is more energetically favorable. However, the qubit transition step center (the flux bias where the population is 0.5, marked by the left dotted line) is shifted away from the symmetry position of the energy spectrum (the zero flux detuning point, identified as the midpoint of the resonant peak/dip positions) by an amount about 29 mΦ_0. This deviation can be attributed to the coupling between the qubit loop and the readout dc-SQUID loop through the mutual inductance. As we performed the state readout, the phase bias of the qubit was changed by the circulating current in the readout dc-SQUID loop and thus the qubit step center does not coincide with the spectrum center.[4] When applying a microwave with frequency 17.0 GHz and nominal power −16 dB m, we observed the resonant peaks/dips on the qubit transition step. The resonant peaks (dips) reflect the microwave induced excitation from flux state $|R\rangle$ to $|L\rangle$ ($|L\rangle$ to $|R\rangle$). The width of the resonant peaks/dips is generally on the order of several mΦ_0, based on which one can estimate the system decoherence time to be less than 1 ns.[20] Another noticeable feature is the strong population inversion, suggesting that higher energy levels other than the first two lowest states are involved.[18]

Then in Fig. 2(b) we plotted the qubit population in $|L\rangle$ state as a function of the nominal microwave power at a fixed flux detuning $\delta\Phi_f^q = 3$ mΦ_0 [marked by the right dashed line in Fig. 2(a)]. The population exhibits a damped oscillation around 0.5. This is different from a good Bessel function dependence as that observed in a superconducting persistent-current qubit.[14] A simple model may address this difference. In our experiments, due to the short decoherence time, a high-frequency field was applied in order to get clear interference fringes. Consequently large amplitude must be applied in order to observe a full modulation period of the interference for a high-frequency field. However, for a very large microwave power, other excitations besides LZ transitions can occur. Figure 2(c) illustrates various transitions in a tilted double-well potential of an rf-SQUID qubit. The system has a few quantized levels that are below the barrier and localized in corresponding potential well. The qubit is assumed to be initially in $|0R\rangle$, i.e., the ground state of right well. When the microwave power is not very large (i.e., the double-well potential always holds), the LZ transitions (with rate W) between $|0R\rangle$ and $|nL\rangle$ (the nth excited state of left well), and the fast intrawell relaxation (with rate γ) from $|nL\rangle$ to $|0L\rangle$ dominate the dynamics of the qubit population. These processes can generate population inversion and lead to a nonmonotonic dependence of qubit population on microwave power. With microwave power increasing, the qubit has probability to be directly excited from the ground state to a higher energy level $|N\rangle$ (with rate g), which is above the top of the barrier and has a nonlocal wave function spanning in both potential wells. The qubit in $|N\rangle$ can relax quickly back to the ground states ($|0L\rangle$ and $|0R\rangle$) of both wells with
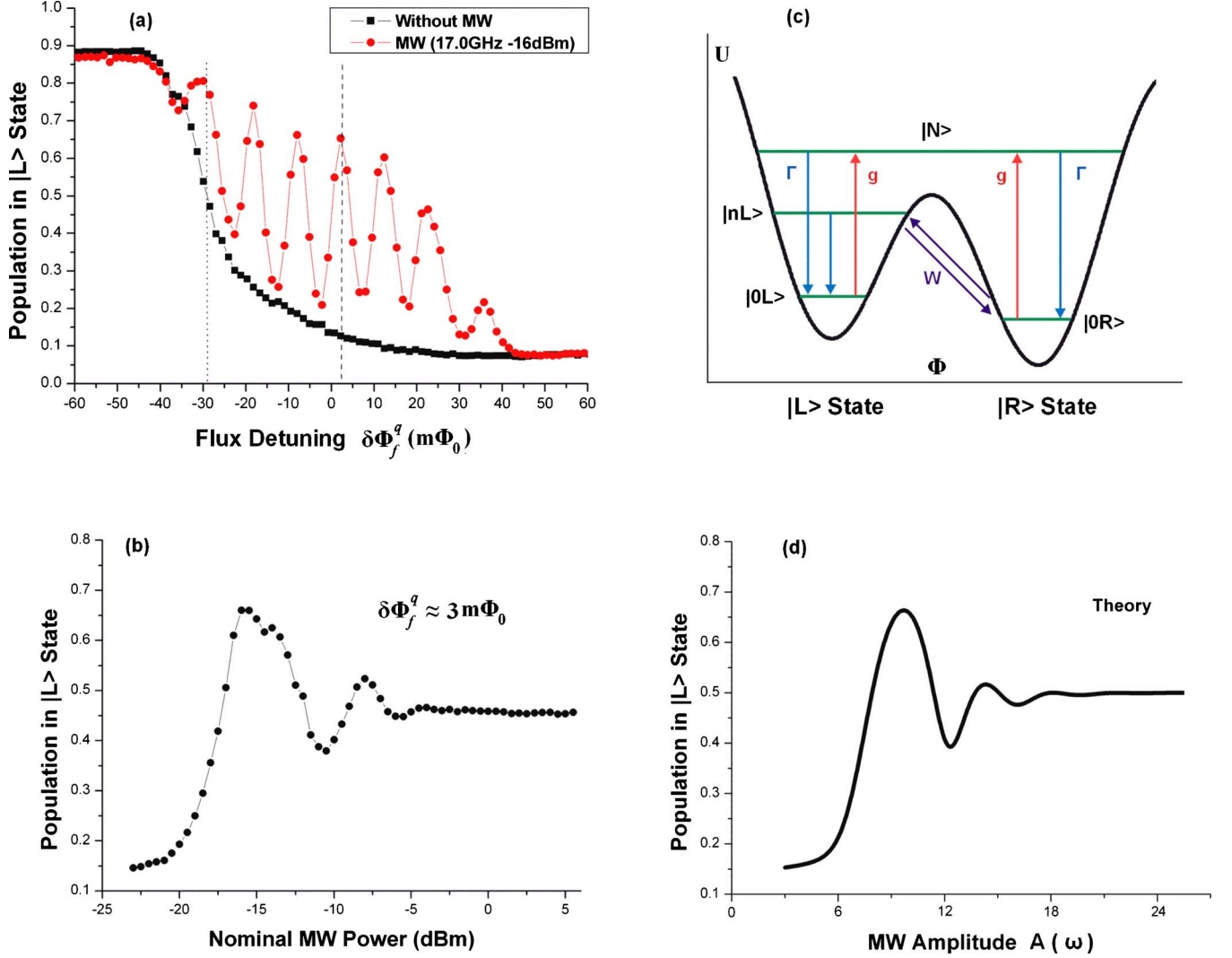
FIG. 2. (Color online) (a) Normalized qubit population in $|L\rangle$ state as a function of dc flux detuning Φ_f^q. As a guide to eyes, the left dotted line marks the qubit transition step center where the population is 0.5 in the absence of microwave. Four peaks and dips (symmetric about the zero flux detuning position, i.e., the spectrum center) are induced by a 10 μs microwave pulse at 17.0 GHz and -16 dB m. A resonant peak with strong population inversion was observed around a dc flux detuning $\delta\Phi_f^q = 3$ mΦ_0, marked with dashed line. (b) Normalized qubit population in $|L\rangle$ state versus the nominal microwave power at a fixed dc flux detuning 3 mΦ_0. (c) An illustration of double-well potential at a fixed flux detuning and the relevant transition processes involved in Fig. 2(b). $|0R\rangle$ and $|0L\rangle$ are the ground states of right well and left well respectively. $|nL\rangle$ is the nth excited state in the left well. $|N\rangle$ represents a higher energy level which is not localized in either potential well. The red (blue) lines show the excitation (relaxation) path. The purple lines represent the LZ transitions between $|0R\rangle$ and $|nL\rangle$. $n=4$ in our following calculation. (d) Calculated qubit population in $|L\rangle$ state as a function of microwave amplitude. The relevant parameters used in our theoretical model are: $\omega/2\pi=17$ GHz, $m=8$, $\Delta/2\pi=7$ MHz, $\Gamma_2/2\pi=2$ GHz, $\gamma/2\pi=\Gamma/2\pi=2$ GHz, $\Gamma_{10}/2\pi=0.6$ kHz, $\Gamma_{01}/2\pi=0.1$ kHz, $a/2\pi=5$ Hz, $b=1.4$.

an approximately equal relaxation rate Γ. Therefore this process equalizes the qubit population in the two wells. Taking all these transition processes into consideration, one can obtain the rate equations to describe the qubit level occupations p_i ($i=0,1,2,3$, corresponding to $|0R\rangle$, $|0L\rangle$, $|nL\rangle$, and $|N\rangle$, respectively) as

$$\dot{p}_0 = -(W + g + \Gamma_{01})p_0 + \Gamma_{10}p_1 + Wp_2 + \Gamma p_3,$$

$$\dot{p}_1 = \Gamma_{01}p_0 - (g + \Gamma_{10})p_1 + \gamma p_2 + \Gamma p_3,$$

$$\dot{p}_2 = Wp_0 - (W + \gamma)p_2,$$

$$p_0 + p_1 + p_2 + p_3 = 1. \tag{1}$$

Under the assumption of classical noise and using perturbation theory, the LZ transition rate between $|0R\rangle$ and $|nL\rangle$ takes the form[17]

$$W(\epsilon, x) = \frac{\Delta^2}{2} \sum_m \frac{\Gamma_2 J_m^2(x)}{(\epsilon - m\omega)^2 + \Gamma_2^2}, \tag{2}$$

where Δ is the avoided crossing between $|0R\rangle$ and $|nL\rangle$, ϵ is the dc energy detuning from the avoided crossing Δ, and $\Gamma_2 = 1/T_2$ is the system dephasing rate. $J_m(x)$ are Bessel func-

tions of the first kind with the argument $x = A/\omega$, where A and ω are field amplitude and frequency, respectively. For a m photon on resonance transition process, $\epsilon = m\omega$.

The transition rate from the ground state to $|N\rangle$ is sensitive to the barrier height during the microwave driving process. We simply assumed the transition rate has an exponential dependence on field amplitude A, i.e., $g = ae^{bA}$, where a, b are two fitting parameters. Γ_{10} (Γ_{01}) is the slow interwell relaxation rate between $|0L\rangle$ and $|0R\rangle$. In the stationary case, $\dot{p}_0 = \dot{p}_1 = \dot{p}_2 = \dot{p}_3 = 0$, Eq. (1) can be solved numerically with appropriate model parameters. Figure 2(d) shows the calculated qubit population of state $|L\rangle$ as a function of the microwave amplitude. The theoretical curve clearly exhibits the main features of the experimental results, indicating that our model captures the underlying physics. We would like to mention that the difference units were used for the horizontal axis. The reason is that we are not able to accurately determine the actual circuit attenuation as well as the mutual inductance between the qubit and microwave line. Then we are not able to determine the actual microwave amplitude applying to the qubit loop.

Figure 3(a) shows the contour plot of the qubit population in state $|L\rangle$ versus the dc flux detuning $\delta\Phi_f^q$ and the nominal microwave power with a fixed microwave frequency at 17.0 GHz. According to the previous works,[14] one expected that the resonant peaks are equally spaced on the flux detuning axis, the distance between adjacent peaks is proportional to the frequency, and the interference fringes follow a Bessel function dependence along the microwave amplitude axis. However, here we observed two sets of resonant peaks. The first set includes four resonant peaks, locating around flux detuning 3 mΦ_0, 12 mΦ_0, 23 mΦ_0, and 37 mΦ_0, respectively [marked by four upward red arrows from left to right in Fig. 3(a)]. The second set lies in the higher microwave power region and includes three resonant peaks, locating around flux detuning 10 mΦ_0, 22 mΦ_0, and 38 mΦ_0 (marked by three downward black arrows). We can group them into two sets because as microwave frequency varied, the resonance positions moved with two different energy-spectrum slopes, indicating the presence of two different transition paths. Moreover, the flux spacing between the resonant peaks of both sets increases with increasing flux detuning and the two sets of interference fringes have overlap along microwave power axis. Therefore, the interference pattern looks complicated and is very different from the regular patterns induced by Landau-Zener transition.[11–15,18]

In order to explain the interference patterns we have to deal with a multilevel system. Since the potential barrier of the rf-SQUID qubit is high, the Landau-Zener transition rate is low for the lower energy states. We thereby consider the avoided crossings close to the top of the barrier and the principle is qualitatively illustrated in Fig. 3(b). Assuming that without microwave the qubit is initially in state $|0R\rangle$ at a fixed dc flux detuning $\delta\Phi_f^q$. The first set of interference fringes is associated with LZ transitions at level crossing $\Delta_{0R,nL}$, opened by the ground state of right well and the nth excited state of left well. One should note that another avoid crossing $\Delta_{0L,nR}$ at positive flux detuning is also present but not shown in Fig. 3(a) for simplicity. The red path represents the main transition processes for generating the first set of
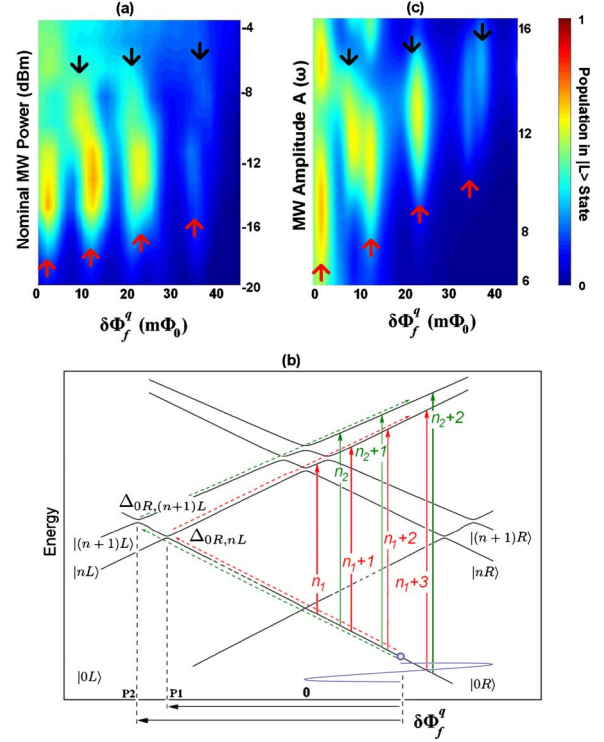

FIG. 3. (Color online) (a) Dependence of qubit population in $|L\rangle$ state on dc flux detuning $\delta\Phi_f^q$ and nominal microwave power, with microwave frequency at 17.0 GHz. Part of two sets of overlapped interference fringes can be observed and population inversion is clearly demonstrated. (b) Energy-level diagram illustrating the multiphoton transition processes. The qubit is initially dc biased at $\delta\Phi_f^q$, where the ground state is $|0R\rangle$. Microwave consecutively drives the qubit through the energy levels that are approximately linear in flux detuning and LZ transitions occur at the avoided level crossings $\Delta_{0R,nL}$ and $\Delta_{0R,(n+1)L}$. The positions of the two level crossings are marked by P1 and P2 (P1 = −45 mΦ_0 and P2 = −56 mΦ_0 in our simulation). The red and green paths, with different energy-level slope, represent the main processes to generate the first and second interference set, respectively. (c) Numerically simulated qubit population in $|L\rangle$ state versus flux detuning and microwave amplitude. The calculated interference patterns show good agreement with the experimental observations [Fig. 3(a)].

interference fringes. The second set of interference fringes is associated with LZ transitions at a nearby level crossing $\Delta_{0R,(n+1)L}$ (also $\Delta_{0L,(n+1)R}$) and the green path represents the main transition processes for generating them. The four peaks in the first set of interference fringes correspond to n_1 photon and up to (n_1+3)-photon transitions and the three peaks in the second set of interference fringes correspond to n_2 photon and up to (n_2+2)-photon transitions. According to the energy spectrum, the slope of the green path is smaller than that of the red path. Therefore the flux spacing of the resonant peaks of the second set of interference fringes is larger than that of the first set. With increasing flux detuning, the energy spectrum becomes flattened, leading to the increase of flux spacing of the resonant peaks. The overlap of these two sets of resonant peaks along power axis can also be understood from Fig. 3(b). The appearance of the first set of interference fringes corresponds to a microwave amplitude,

which can make the qubit flux bias reach the first level crossing position (P1). For a high-frequency microwave, the consecutive nodes of the Bessel function of the interference fringe can span in a wide range of microwave power. Therefore, in the oscillatory period of the first interference set, the second level crossing (P2) can be easily reached and then the second interference set starts to show up. This feature is very different from the observation of well-resolved individual interference diamonds when applying a relatively low-frequency microwave.

To quantitatively understand the experimental results, we performed numerical calculation based on the rate equation approach introduced in Ref. 21. In our calculation, the relevant six energy levels shown in Fig. 3(b) were taken into account. For convenience, we use $|0\rangle$, $|1\rangle$, $|2\rangle$, $|3\rangle$, $|4\rangle$, and $|5\rangle$ to denote flux states $|0R\rangle$, $|0L\rangle$, $|nR\rangle$, $|nL\rangle$, $|(n+1)R\rangle$, and $|(n+1)L\rangle$, respectively. $\Delta_{0R,nL}$ and $\Delta_{0R,(n+1)L}$ are also denoted by Δ_1 and Δ_2. Then we can write down the rate equations to describe the qubit level occupations $p_i(i=0,1,2,3,4,5)$ as

$$\dot{p}_0 = -(W_{03} + W_{05} + \Gamma_{01})p_0 + \Gamma_{10}p_1 + \Gamma(p_2 + p_4) + W_{30}p_3$$
$$+ W_{50}p_5,$$

$$\dot{p}_1 = \Gamma_{01}p_0 - (W_{12} + W_{14} + \Gamma_{10})p_1 + \Gamma(p_3 + p_5) + W_{21}p_2$$
$$+ W_{41}p_4,$$

$$\dot{p}_2 = W_{12}p_1 - (W_{21} + \Gamma)p_2,$$

$$\dot{p}_3 = W_{03}p_0 - (W_{30} + \Gamma)p_3,$$

$$\dot{p}_4 = W_{14}p_1 - (W_{41} + \Gamma)p_4,$$

$$p_0 + p_1 + p_2 + p_3 + p_4 + p_5 = 1, \tag{3}$$

where W_{ij} are the LZ transitions between states $|i\rangle$ and $|j\rangle$, which can be explicitly written as

$$W_{03} = W_{30} = W_{12} = W_{21} = \frac{\Delta_1^2}{2} \sum_m \frac{\Gamma_2 J_m^2(x)}{(\epsilon_1 - m\omega)^2 + \Gamma_2^2},$$

$$W_{05} = W_{50} = W_{14} = W_{41} = \frac{\Delta_2^2}{2} \sum_m \frac{\Gamma_2 J_m^2(x)}{(\epsilon_2 - m\omega)^2 + \Gamma_2^2}, \tag{4}$$

where ϵ_1 and ϵ_2 are the dc energy detuning from the avoided crossing Δ_1 and Δ_2 respectively. Γ is the fast intrawell relaxation rate and Γ_{10} (Γ_{01}) is the slow interwell relaxation rate between $|1\rangle$ and $|0\rangle$. In the stationary case, $\dot{p}_0 = \dot{p}_1 = \dot{p}_2 = \dot{p}_3 = \dot{p}_4 = \dot{p}_5 = 0$. In our calculation, $\omega/2\pi = 17$ GHz, $n = 4$, $n_1 = 8$, $n_2 = 10$, $\Delta_{0R,4L}/2\pi = \Delta_1/2\pi = 7$ MHz, $\Delta_{0R,5L}/2\pi = \Delta_2/2\pi = 13$ MHz. As shown in Fig. 3(b), these model parameters can fully describe the energy-level structure and correspond to the following sample parameters: qubit loop inductance $L \approx 1.3$ nH, junction capacitance $C \approx 35$ fF and junction critical current $I_c \approx 610$ nA. We obtained the qubit inductance from its geometrical size and determined the capacitance based on the independent macroscopic quantum tunneling data. The junction critical current was the main fitting parameter in our simulation. Other relevant fitting param-

eters in calculation are: $\Gamma_2/2\pi = 2$ GHz, $\Gamma/2\pi = 2$ GHz. Γ_{10} (Γ_{01}) was assumed to have an exponential dependence on the flux bias and the fitting values are on the same order of those obtained from independent measurements. By using the above parameters and taking into account the different energy-level slopes for different transition paths, one can numerically solve Eq. (4) in the stationary case and obtains the qubit population in $|L\rangle$ state as a function of the microwave amplitude and dc flux detuning, as shown in Fig. 3(c). The agreement between experimental results and numerical calculation is good. In our simulation, we did not consider the nonadiabatic state excitations within the same well. We simply used the adiabatic picture, which is valid for field driving with frequency much smaller than the relevant energy-level separation. However, the MW frequency in our experiment was close to the energy difference between discreet quantum states in the same well. Taking this nonadiabatic effect into account we should better understand the experiments.

As shown by LZ transition rate expression Eq. (2), the magnitude of LZ transition rate depends crucially on the tunneling splitting Δ, which is an exponential function of the potential barrier height. In the experiment, there is an observable window for the LZ transitions. If Δ is too large, the system relaxes to the ground state too fast that one cannot obtain clear interference patterns. On the contrary, if Δ is too small, no state transitions happen in an acceptable measurement cycle. Therefore, the measured LZ interference patterns can be very different for various sample parameters. Furthermore, due to the large size, the rf-SQUID qubit usually has much shorter decoherence time than that of the superconducting persistent-current qubit. In order to resolve clear interference patterns, one has to apply microwave with high frequency and large power, which will lead excitation to many higher energy levels. Although the contribution from high levels complicates the interference patterns, we can still quantitatively understand the interference using LZ transitions. A detailed theoretical discussion on the interference features with large-amplitude and high-frequency field can be found in Ref. 22.

In conclusion, we observed the quantum interference fringes in a superconducting rf-SQUID qubit driven by large-amplitude and high-frequency microwave field. The interference pattern exhibits two sets of overlapped resonant peaks with well-resolved multiphoton transitions. The two sets of interference fringes correspond to two different transition paths associated with LZ transitions at two consecutive level crossing. We developed a theoretical model involving the relevant energy levels near and above the top of the energy barrier between the potential wells and numerically simulated interference patterns. The agreement between the simulation and experimental results reflects the nature of multi-level excitation in the rf-SQUID qubit under strong microwave driving.

*gzsun@nju.edu.cn

†yuyang@nju.edu.cn

[1] Y. Nakamura, Yu. A. Pashkin, and J. S. Tsai, Phys. Rev. Lett. **87**, 246601 (2001).

[2] D. Vion, A. Aassime, A. Cottet, P. Joyez, H. Pothier, C. Urbina, D. Esteve, and M. H. Devoret, Science **296**, 886 (2002).

[3] Y. Yu, S. Han, X. Chu, S. Chu, and Z. Wang, Science **296**, 889 (2002).

[4] I. Chiorescu, Y. Nakamura, C. J. P. M. Harmans, and J. E. Mooij, Science **299**, 1869 (2003).

[5] S. Saito, T. Meno, M. Ueda, H. Tanaka, K. Semba, and H. Takayanagi, Phys. Rev. Lett. **96**, 107001 (2006).

[6] J. Lisenfeld, A. Lukashenko, M. Ansmann, J. M. Martinis, and A. V. Ustinov, Phys. Rev. Lett. **99**, 170504 (2007).

[7] A. V. Shytov, D. A. Ivanov, and M. V. Feigel'man, Eur. Phys. J. B. **36**, 263 (2003).

[8] S. N. Shevchenko, A. S. Kiyko, A. N. Omelyanchouk, and W. Krech, Low Temp. Phys. **31**, 569 (2005).

[9] E. C. G. Stuckelberg, Helv. Phys. Acta **5**, 369 (1932).

[10] N. F. Ramsey, Phys. Rev. **76**, 996 (1949).

[11] M. Sillanpää, T. Lehtinen, A. Paila, Y. Makhlin, and P. Hakonen, Phys. Rev. Lett. **96**, 187002 (2006).

[12] A. Izmalkov, S. H. W. van der Ploeg, S. N. Shevchenko, M. Grajcar, E. Il'ichev, U. Hubner, A. N. Omelyanchouk, and H.-G.

Meyer, Phys. Rev. Lett. **101**, 017003 (2008).

[13] S. N. Shevchenko, S. H. W. van der Ploeg, M. Grajcar, E. Il'ichev, A. N. Omelyanchouk, and H.-G. Meyer, Phys. Rev. B **78**, 174527 (2008).

[14] W. D. Oliver, Y. Yu, J. C. Lee, K. K. Berggren, L. S. Levitov, and T. P. Orlando, Science **310**, 1653 (2005).

[15] D. M. Berns, W. D. Oliver, S. O. Valenzuela, A. V. Shytov, K. K. Berggren, L. S. Levitov, and T. P. Orlando, Phys. Rev. Lett. **97**, 150502 (2006).

[16] D. M. Berns, M. S. Rudner, S. O. Valenzuela, K. K. Berggren, W. D. Oliver, L. S. Levitov, and T. P. Orlando, Nature (London) **455**, 51 (2008).

[17] M. S. Rudner, A. V. Shytov, L. S. Levitov, D. M. Berns, W. D. Oliver, S. O. Valenzuela, and T. P. Orlando, Phys. Rev. Lett. **101**, 190502 (2008).

[18] G. Sun, X. Wen, Y. Wang, S. Cong, J. Chen, L. Kang, W. Xu, Y. Yu, S. Han, and P. Wu, Appl. Phys. Lett. **94**, 102502 (2009).

[19] G. Sun, J. Chen, Z. Ji, W. Xu, L. Kang, P. Wu, N. Dong, G. Mao, Y. Yu, and D. Xing, Appl. Phys. Lett. **89**, 082516 (2006).

[20] C. H. van der Wal, A. C. J. ter Haar, F. K. Wilhelm, R. N. Schouten, C. J. P. M. Harmans, T. P. Orlando, S. Lloyd, and J. E. Mooij, Science **290**, 773 (2000).

[21] X. Wen and Y. Yu, Phys. Rev. B **79**, 094529 (2009).

[22] X. Wen, Y. Wang, and Y. Yu, arXiv:0912.0881 (unpublished).